

Communication

Energy-Resolved Ultrafast Spectroscopic Investigation on the Spin-Coupled Electronic States in Multiferroic Hexagonal HoMnO₃

Wei-Hong Huang ^{1,†} , Hao-Keng Wei ^{1,†}, Nguyen Nhat Quyen ¹ , Pei-Tsung Yang ¹, Yi-Cheng Cheng ¹, Yu-Ting Wang ¹, Ying-Kuan Ko ¹, Chien-Ming Tu ^{1,*}, Atsushi Yabushita ¹ and Chih-Wei Luo ^{1,2,3,4,*} 

- ¹ Department of Electrophysics, National Yang Ming Chiao Tung University, Hsinchu 300093, Taiwan; nc7410.sc05@nycu.edu.tw (W.-H.H.); ihatotomato.sc05@nycu.edu.tw (H.-K.W.); nhatquyen126.sc06@nycu.edu.tw (N.N.Q.); crocin201@gmail.com (P.-T.Y.); allen8612231997@gmail.com (Y.-C.C.); wongmom152@yahoo.com.tw (Y.-T.W.); kentko78@gmail.com (Y.-K.K.); yabushita@nycu.edu.tw (A.Y.)
- ² Institute of Physics and Center for Emergent Functional Matter Science, National Yang Ming Chiao Tung University, Hsinchu 300093, Taiwan
- ³ National Synchrotron Radiation Research Center, Hsinchu 30076, Taiwan
- ⁴ Taiwan Consortium of Emergent Crystalline Materials, Ministry of Science and Technology, Taipei 10601, Taiwan
- * Correspondence: cmtu@nycu.edu.tw (C.-M.T.); cwluoep@nycu.edu.tw (C.-W.L.)
- † These authors contributed equally to this work.



Citation: Huang, W.-H.; Wei, H.-K.; Quyen, N.N.; Yang, P.-T.; Cheng, Y.-C.; Wang, Y.-T.; Ko, Y.-K.; Tu, C.-M.; Yabushita, A.; Luo, C.-W. Energy-Resolved Ultrafast Spectroscopic Investigation on the Spin-Coupled Electronic States in Multiferroic Hexagonal HoMnO₃. *Materials* **2022**, *15*, 5188. <https://doi.org/10.3390/ma15155188>

Academic Editors: Lado Filipovic and Tibor Grasser

Received: 19 June 2022

Accepted: 25 July 2022

Published: 26 July 2022

Publisher's Note: MDPI stays neutral with regard to jurisdictional claims in published maps and institutional affiliations.



Copyright: © 2022 by the authors. Licensee MDPI, Basel, Switzerland. This article is an open access article distributed under the terms and conditions of the Creative Commons Attribution (CC BY) license (<https://creativecommons.org/licenses/by/4.0/>).

Abstract: A complete temperature-dependent scheme of the Mn³⁺ on-site d-d transitions in multiferroic hexagonal HoMnO₃ (*h*-HoMnO₃) thin films was unveiled by energy-resolved ultrafast spectroscopy. The results unambiguously revealed that the ultrafast responses of the *e*_{1g} and *e*_{2g} states differed significantly in the hexagonal HoMnO₃. We demonstrated that the short-range antiferromagnetic and ferroelectric orderings are more relevant to the *e*_{2g} state, whereas the long-range antiferromagnetic ordering is intimately coupled to both the *e*_{2g} and *e*_{1g} states. Moreover, the primary thermalization times of the *e*_{2g} and *e*_{1g} states were 0.34 ± 0.08 ps and 0.38 ± 0.08 ps, respectively.

Keywords: multiferroic manganites; antiferromagnetic ordering; ferroelectric ordering; ultrafast spectroscopy

1. Introduction

The emergent physical properties resulting from the coupled ferroic orders in multiferroic manganites and their potential applications have attracted considerable research interest [1,2]. In rare-earth manganites, hexagonal RMnO₃ structures with small R³⁺ ions (In, Sc, Y, and the lanthanum atoms from Dy to Lu) exhibit coexisting coupled ferroelectric (FE) and antiferromagnetic (AFM) orders [3,4]. In hexagonal HoMnO₃ (*h*-HoMnO₃), ferroelectricity occurs below the Curie temperature *T*_C (870 K) because structural distortion takes place during the transition from the *P*_{63/*mmc*} to the *P*_{63*cm*} symmetry, as well as the polarization associated with the bonds of Ho and planar oxygen [5]. In *P*_{63*cm*} hexagonal manganites, each Mn³⁺ ion is surrounded by five O²⁻ ions, forming triangular planar sub-lattices in the basal plane (*ab*-plane). The magnetic order of Mn³⁺ is mainly dominated by antiferromagnetic planar Mn – O – Mn superexchange interactions [6,7]. The AFM spin ordering on the high-spin Mn³⁺ ions occur at the Néel temperature *T*_N (76 K). The symmetry of the short-range AFM order of the hexagonal HoMnO₃ has been derived by second harmonic generation (SHG). Below *T*_N, the symmetry of the AFM phase is *P*_{63*cm*} and experiences a sudden rotation by an angle of 90° to *P*_{63*cm*} at around 40 K [8].

Hexagonal HoMnO₃ structures comprise layers of bipyramid MnO₅ separated by layers of Ho³⁺ ions along the *c*-axis. The Mn³⁺ ions are located near the center of the

MnO₅ bipyramids, forming triangular planar sublattices along the *ab*-plane. Because of the crystal field of the bipyramid structure, the *3d*-orbital state of the Mn³⁺ ions split into lower-lying doublet states *e*_{1g} (*d*_{*yz*}/*d*_{*zx*}) and *e*_{2g} (*d*_{*xy*}/*d*_{*x²-y²*}) and an upper-lying singlet state *a*_{1g} (*d*_{*3z²-r²*}) [9], as shown in the inset of Figure 1. Therefore, the four *d* electrons of Mn³⁺ in the ground state occupy *e*_{1g} and *e*_{2g} and leave *a*_{1g} vacant. Previous studies have determined the band structure of the Mn³⁺ *d* orbits in RMnO₃ (*R* = Gd, Tb, Dy, Ho, Er, and Lu) by using optical absorption spectroscopy [9–13]. The absorption spectrum exhibits two peaks around 1.7 and 2.2 eV corresponding to the transitions from *e*_{2g} to *a*_{1g} and *e*_{1g} to *a*_{1g}, respectively, in the on-site Mn³⁺. In addition, the short-range AFM ordering leads to a blue shift in the absorption peaks as the temperature decreases, which further induces a marked change near *T*_N. The indirect exchange interactions, including double-exchange [14], superexchange [15], and super-superexchange [6], play a key role in explaining the spin-ordering in manganite [16]. Specifically, the magnetic exchange interaction between the Mn³⁺ ions induce the anomalous shift of Mn *d* levels, indicating a strong correlation between the electronic structure and spin ordering [10,12]. Moreover, in addition to hexagonal manganites exhibiting large atomic displacements at *T*_N [17,18], the optical phonon frequency also shows an unexpected shift because of the magnetic ordering [19–21]. The large atomic displacements combined with phonon anomalies further demonstrate the coupling between the magnetic order and electric dipole moments through the lattice. Accordingly, multiferroic manganites exhibit an intimate coupling between the charge, lattice, and spin degrees of freedom.

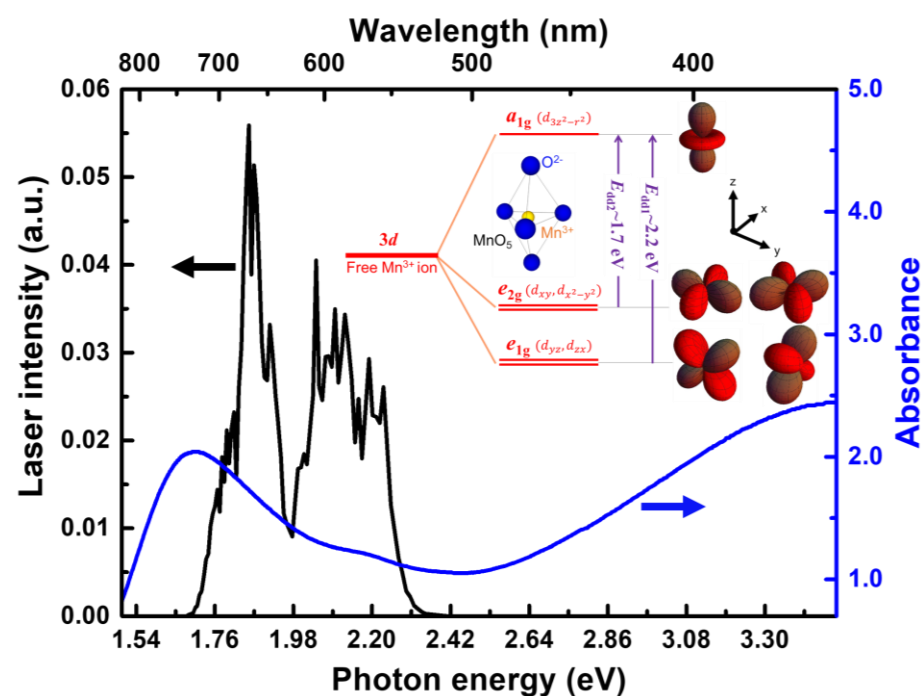


Figure 1. Stationary absorption spectrum of a hexagonal HoMnO₃ thin film and the laser spectrum used in this study. The inset shows the electronic levels of the five-fold coordinated Mn³⁺ ion in the MnO₅ trigonal bipyramidal field of the five surrounding O²⁻ ligands.

Time-resolved optical pump-probe spectroscopy is effective for demonstrating and quantifying the interaction strength among quasiparticles and various degrees of freedom [22–26]. This technique has been extensively employed to identify the underlying physical mechanisms of hexagonal manganites [27–31]. However, most previous studies on transient spectroscopy have focused only on the dynamics of the *e*_{2g} state, and the other unobservable Mn³⁺ *d* orbits remain unclear. In the present study, we adopted an advanced ultrafast spectroscopy technique that involved using a broadband and ultrashort pulse

laser to comprehensively examine the complete temperature-dependent scheme of the Mn^{3+} on-site $d-d$ transitions in rare-earth multiferroic hexagonal manganite HoMnO_3 .

2. Materials and Methods

The samples used in this study were hexagonal c -axis HoMnO_3 thin films with a thickness of 180 nm. The films were deposited on double-sided polished yttria-stabilized zirconia (111) substrates through pulsed-laser (KrF excimer laser) deposition [28]. The thin films were employed to measure both the stationary and transient spectra in a transmissivity configuration to obtain high-quality data. Figure 1 shows the stationary absorption spectrum of the hexagonal HoMnO_3 thin film measured at room temperature. The absorption spectrum clearly shows the Mn^{3+} $d-d$ transition around 1.7 eV (e_{2g} to a_{1g} , E_{dd2}) and 2.2 eV (e_{1g} to a_{1g} , E_{dd1}). The transition peak centered at about 1.7 eV is consistent with previous optical absorption spectra in hexagonal-phase RMnO_3 ($R = \text{Gd, Tb, Dy, Ho, Er,}$ and Lu) [9–13]. The other hidden $d-d$ transition around 2.2 eV, which is embedded in the substantially more intense absorption peak, was verified using second-harmonic generation [8,13,32]. To simultaneously reveal the strongly AFM- and temperature-dependent Mn^{3+} $d-d$ transitions (i.e., E_{dd1} and E_{dd2}), a light source with a broad spectrum in the visible range is required [33]. The time-resolved spectroscopic measurements in this study were based on 10 fs visible pulses generated by a noncollinear optical parametric amplifier (NOPA) [34,35]. A generative amplifier (800 nm, 5 kHz, 1.8 W, Legend-USP-HE; Coherent, Santa Clara, CA, USA) seeded with a Ti:sapphire laser oscillator (Micra 10; Coherent) was used as the pump source of the NOPA. Figure 1 shows that the laser spectrum (1.7–2.3 eV) covered the targeted whole Mn^{3+} $d-d$ transition bands. For the pump-probe measurements, a beam splitter splits the visible pulses into pump and probe beams with the same spectrum. The fluences of pump and probe were 0.85 and 0.07 mJ/cm^2 , respectively, and focused on the samples. The normalized transient transmittance changes $\Delta T/T$ (ΔT : the transmittance changes induced by the pump pulses; T : the transmittance of the probe pulses) spectra were captured using a wavelength-resolved multichannel lock-in amplifier as a function of delay time between pump and probe pulses [36].

3. Results and Discussion

Figure 2a,b display the two-dimensional (2D) plots of the relative transient transmittance change ($\Delta T/T$) spectra as functions of the probe photon energy and delay time at temperatures above ($T = 100$ K) and below ($T = 35$ K) T_N . In the 2D plots, the black lines represent the borders of the positive and negative components of the $\Delta T/T(v, t)$ signals. The temperature dependence of the positive $\Delta T/T$ signal in the range of approximately 1.7–2.3 eV was attributed to photobleaching resulting from the depletion of the initial state and the population of the excited state, indicating the $d-d$ transitions of E_{dd1} and E_{dd2} . As a result, the energy dependence of the positive $\Delta T/T$ signals (in Figure 2c) is similar to that of the stationary absorption spectrum shown in Figure 1. By contrast, the induced absorption to the higher excited states resulted in a negative $\Delta T/T$ signal in the blocked-photon energy range, which did not correspond to the on-site Mn^{3+} $d-d$ transition bands. Therefore, the zero-amplitude position distinctly indicated the boundary of the $d-d$ transitions E_{dd1} and E_{dd2} as the solid black lines in Figure 2a,b. The transition band edges E_{dd1} and E_{dd2} were extracted to further investigate the transient dynamics of the Mn^{3+} d bands at various temperatures, as shown in Figure 3, and both transition bands E_{dd1} and E_{dd2} clearly exhibited blue shift when the temperature decreased. Furthermore, in addition to the monotonic blue shift, the transient curves revealed the significant characteristics within the short period at temperatures below T_N .

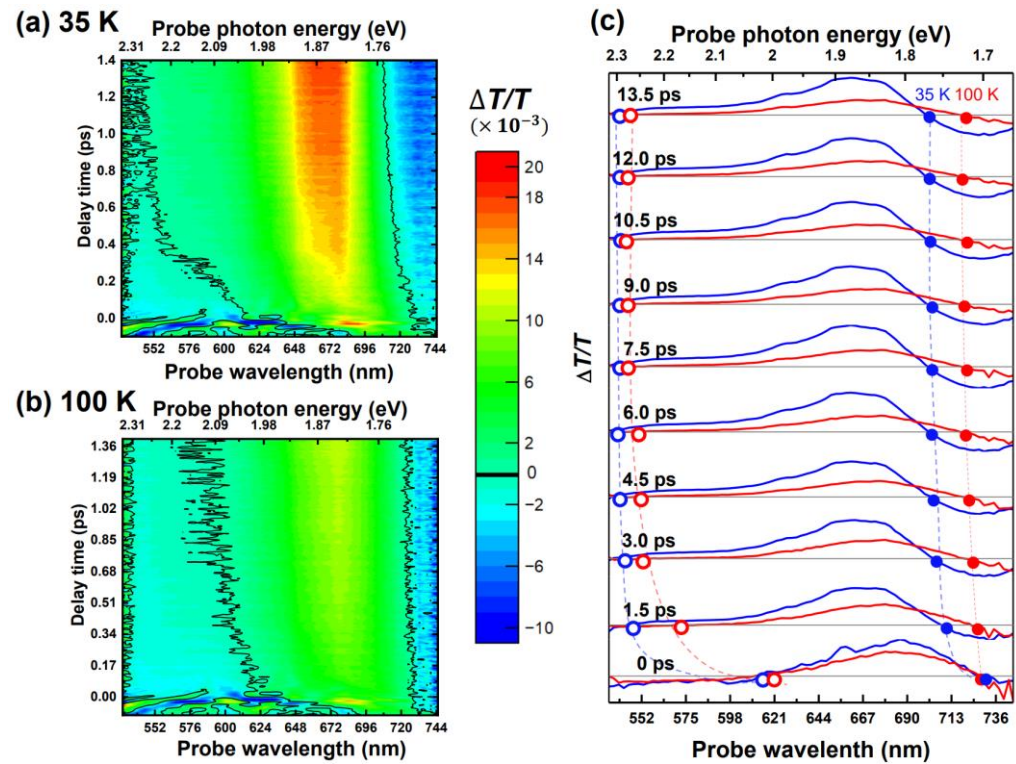


Figure 2. (a,b) Two-dimensional plots of the transient difference transmittance $\Delta T/T$ at temperatures below (35 K) and above (100 K) T_N . (c) Time-resolved $\Delta T/T$ spectra at different delay time between the pump and probe pulses at 35 K (blue) and 100 K (red). The horizontal gray lines show where $\Delta T/T = 0$. The solid and hollow dots represent the boundary of d - d transitions, and the solid and hollow dots respectively indicate the time-resolved E_{dd2} ($e_{2g} \rightarrow a_{1g}$) and E_{dd1} ($e_{1g} \rightarrow a_{1g}$) transitions. The dashed lines are guides for eyes to represent the time evolution of these transitions.

The time-resolved traces of $E_{dd1}(t)$ and $E_{dd2}(t)$ at each photon energy level can be phenomenologically expressed as

$$E(t) = E_1 e^{-\frac{t}{\tau_1}} + E_2 e^{-\frac{t}{\tau_2}} + E_{\text{const}}, \quad (1)$$

where E_i is the amplitude of the exponential function, and τ_i represents the relaxation time for the corresponding component. Figure 4 shows the fitting results (for the detailed fitting results, please see Table S1 in Supplementary Materials). The constant term E_{const} in Figure 4c,f indicates the transition energy level after thermal equilibrium was reached. In consistence with the temperature-dependent stationary absorption spectra in previous studies [10,12], the transition energies shifted and exhibited an anomaly at T_N . In E_{dd2} (see Figure 4d,e), both the amplitudes (E_1 and E_2) and time constants ($\tau_1 = 0.38 \pm 0.08$ ps and 0.95 ± 0.50 ps; $\tau_2 = 2.40 \pm 0.40$ ps and 5.90 ± 0.70 ps; below and above T_N , respectively) exhibited noticeable changes across T_N . On the other hand, the time-dependent E_{dd1} (see Figure 4a,b) differed markedly at temperatures above and below T_N . The fast component τ_1 (0.34 ± 0.08 fs) was observed only at temperatures below T_N , whereas the slow component τ_2 (2.00 ± 0.60 ps) was preserved at all of the measured temperatures.

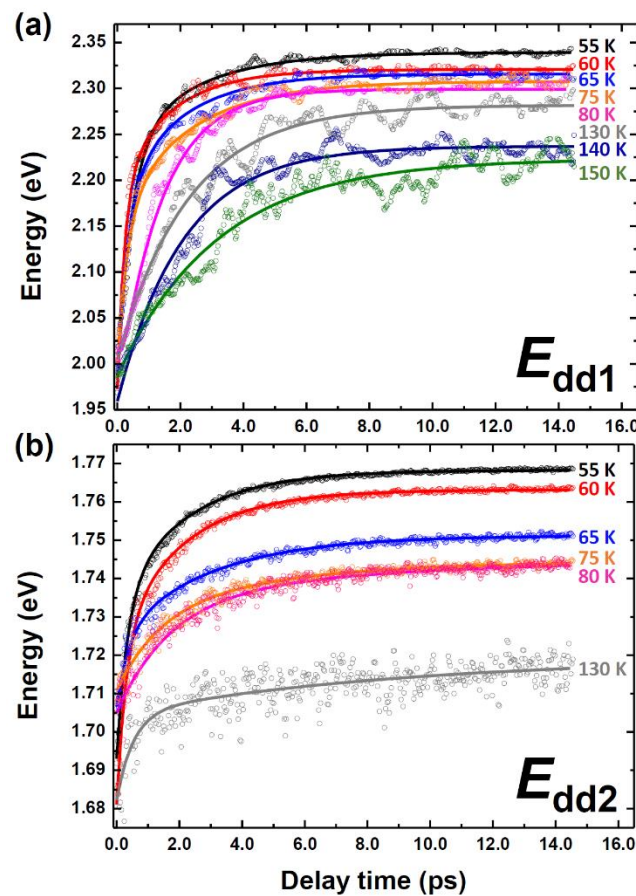


Figure 3. Time evolution of Mn^{3+} on-site $d-d$ transition of (a) E_{dd1} ($e_{1g} \rightarrow a_{1g}$) and (b) E_{dd2} ($e_{2g} \rightarrow a_{1g}$) at different temperatures.

The assignment of the relaxation components in multiferroic materials has been a challenging subject for decades because of the complicated correlations among the electron, lattice, charge polarization, and AFM spin ordering. A previous study [37] attributed a relaxation time of approximately 0.4 ps to phonon thermalization. On the same time scale, Satoh et al. [38] assigned a relaxation time of approximately 0.9 ps to the demagnetization of AFM compounds. Additionally, previous studies have attributed the few-ps component to electron-lattice relaxation [39,40] or spin-lattice relaxation [28]. In this paper, we propose a model based on our results as well as those from previous studies. The few-ps component τ_2 occurred in both E_{dd1} and E_{dd2} at all of the measured temperatures. Thus, the few-ps component τ_2 could be attributed to the relaxation of the excited carriers in a_{1g} , which is the final state of both E_{dd1} and E_{dd2} transitions from the initial states e_{1g} and e_{2g} , respectively. The excited electrons relaxed to the bottom of a_{1g} and banded through the electron-phonon coupling with a few-ps relaxation time, and the transition band exhibited a blue shift induced by the disappearance of the renormalization of the bandgap [41]. This has also been observed in other manganites [27,42]. The significant changes in the amplitudes and relaxation time across T_N indicate an intimate correlation among the electron, lattice, and spin, which corresponds to the sudden shift in the positions of relevant atoms [17,18] and the anomaly in the Raman spectra [19,20] at the spin-ordering temperature.

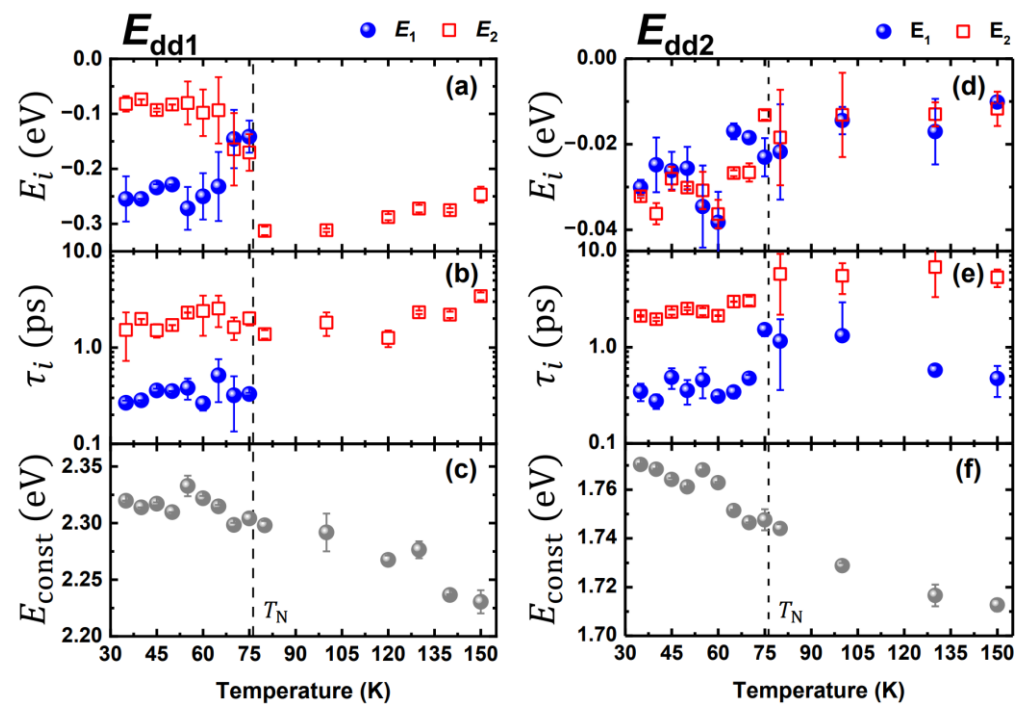


Figure 4. Fitting results of the E_{dd1} ($e_{1g} \rightarrow a_{1g}$) and E_{dd2} ($e_{2g} \rightarrow a_{1g}$) spectra in Figure 3 obtained by using Equation (1). (a,d) Amplitudes E_1 and E_2 , (b,e) relaxation times τ_1 and τ_2 of E_{dd1} and E_{dd2} spectra at various temperatures. (c,f) The constant term of Equation (1) for the energy relaxations in E_{dd1} and E_{dd2} spectra. The black dashed lines indicate T_N .

In contrast, the sub-ps component τ_1 cannot be assigned to population relaxation in the common final state because it exists only in E_{dd2} at high temperatures, as shown in Figure 4b,e. Therefore, the sub-ps component in E_{dd1} and E_{dd2} are ascribed to the relaxation in e_{1g} and e_{2g} , respectively. The e_{2g} state comprises the d_{xy} and $d_{x^2-y^2}$ orbitals, which lie on the basal plane. These orbitals are strongly hybridized with the planar oxygen of the bipyramid structure, indicating a close correlation with the charge-ordering characteristic of the geometric ferroelectricity. Below the FE transition temperature ($T_C = 870$ K in HoMnO_3), the FE moment is along the c -axis between the rare-earth ion (Ho^{3+} in this case) and the planar oxygen on the distorted trigonal bipyramid MnO_5 [5]. Accordingly, the sub-ps lifetime τ_1 is considered to correlate with the destruction of the FE state. Besides, the superexchange in the planar Mn-O-Mn chain combined with the magnetoelastic coupling [17,18] modifies the e_{2g} state and induces a significant difference in both the amplitude and lifetime (including τ_1 and τ_2 in Figure 4d,e) of the pump-probe spectra across T_N , particularly for the sub-ps component τ_1 exhibiting the magnetoelectric coupling. Moreover, this sub-ps (0.38 ± 0.08 ps and 0.95 ± 0.50 ps below and above T_N , respectively) component, which is associated with spin ordering, can be observed at temperatures far above T_N , indicating that the e_{2g} state essentially couples with the short-range AFM spin ordering, which cannot be reliably obtained from standard magnetization measurements. This is in consistency with the previous results of stationary absorption spectra [9–12] and our time-resolved spectroscopies [29,31], which have demonstrated that the e_{2g} state is highly sensitive to short- and long-range AFM spin ordering.

However, the sub-ps component τ_1 can be observed only in the presence of long-range spin ordering in the e_{1g} state (Figure 4b). The e_{1g} state comprises d_{yz} and d_{zx} , which are not as sensitive to the planar oxygen as the e_{2g} state. The time-dependent E_{dd1} shows significant larger fluctuations at temperatures above T_N in Figure 3a. According to a previous study [43] on PL, the electronic transfer from a_{1g} to e_{1g} was strongly blocked by spin fluctuations at temperatures above T_N , indicating that the E_{dd1} is dominated by long-range AFM spin ordering. Therefore, the spin- e_{1g} orbit interaction was attributed as the main

contributor to the sub-ps component in the e_{1g} state [44]. Furthermore, the temperature dependence of the Raman-active phonons, inducing anharmonicity in the A_1 phonon mode (which is the oxygen vibrate along the c -axis) below T_N , indicates that the spin-orbit interaction is strongly influenced by the anisotropic superexchange between the Mn^{3+} and Ho^{3+} ions and the super-superexchange of Mn-O-O-Mn along the c -axis [19,45,46]. This component τ_1 (0.34 ± 0.08 ps) can be ascribed to the thermalization of the spin subsystem in the e_{1g} state.

4. Conclusions

In summary, we have demonstrated that the Mn^{3+} d orbit electronic states are strongly affected by the electric–magnetic coupling in multiferroic h - $HoMnO_3$ thin films. The 2D energy- and time-resolved spectroscopy measurements carried out at various temperatures have unambiguously disclosed the characteristics of Mn^{3+} d orbits. Short-range AFM spin ordering and FE ordering are related to the e_{2g} state. By contrast, long-range AFM spin ordering is strongly coupled to both the e_{2g} and e_{1g} states. The slow electron–phonon relaxation time in the a_{1g} state is 2.70 ± 1.50 ps. Moreover, the depolarization time in the e_{2g} state above T_N is 0.95 ± 0.50 ps, and an anomaly is observed at the AFM spin-ordering temperature, further shortening of the fast relaxation time to 0.38 ± 0.08 ps. In addition, the fast spin-thermalization time caused by the spin-orbit (d_{yz} and d_{zx} orbitals) interaction in the e_{1g} state is 0.34 ± 0.08 ps. Therefore, this study has demonstrated that magnetic ordering in $HoMnO_3$ intimately coupled with the electronic structure of both the e_{1g} and e_{2g} states, respectively, can be investigated using the proposed energy-resolved ultrafast spectroscopy technique.

Supplementary Materials: The following supporting information can be downloaded at: <https://www.mdpi.com/article/10.3390/ma15155188/s1>, Table S1: Fitting results of the E_{dd2} and E_{dd1} spectra in Figure 3 obtained by using Equation (1).

Author Contributions: C.-W.L. proposed the project. Y.-T.W., W.-H.H., H.-K.W., N.N.Q., P.-T.Y., Y.-C.C., Y.-K.K., C.-M.T. and A.Y. performed the experiments and collected the data. All authors have read and agreed to the published version of the manuscript.

Funding: This research was funded by the Ministry of Science and Technology, Taiwan (grant Nos. 109-2112-M-009-020-MY3 and 109-2124-M-009-003-MY3) and the Center for Emergent Functional Matter Science of National Yang Ming Chiao Tung University from The Featured Areas Research Center Program at NYCU within the framework of the Higher Education Sprout Project by the Ministry of Education (MOE) in Taiwan.

Institutional Review Board Statement: Not applicable.

Informed Consent Statement: Not applicable.

Data Availability Statement: Not applicable.

Conflicts of Interest: The authors declare no conflict of interest.

References

1. Nan, C.W.; Bichurin, M.I.; Dong, S.; Viehland, D.; Srinivasan, G. Multiferroic magnetoelectric composites: Historical perspective, status, and future directions. *J. Appl. Phys.* **2008**, *103*, 031101. [[CrossRef](#)]
2. Khomskii, D. Multiferroics: Different ways to combine magnetism and ferroelectricity. *J. Magn. Magn. Mater.* **2006**, *306*, 1–8. [[CrossRef](#)]
3. Prellier, W.; Singh, M.P.; Murugavel, P. The single-phase multiferroic oxides: From bulk to thin film. *J. Phys. Condens. Matter* **2005**, *17*, R803–R832. [[CrossRef](#)]
4. Lorenz, B. Hexagonal Manganites—($RMnO_3$): Class (I) Multiferroics with strong coupling of magnetism and ferroelectricity. *ISRN Condens. Matter Phys.* **2013**, *2013*, 497073. [[CrossRef](#)]
5. Van Aken, B.B.; Palstra, T.T.; Filippetti, A.; Spaldin, N.A. The origin of ferroelectricity in magnetoelectric $YMnO_3$. *Nat. Mater.* **2004**, *3*, 164–170. [[CrossRef](#)]
6. Lonkai, T.; Tomuta, D.G.; Hoffmann, J.-U.; Schneider, R.; Hohlwein, D.; Ihlinger, J. Magnetic two-dimensional short-range order in hexagonal manganites. *J. Appl. Phys.* **2003**, *93*, 8191–8193. [[CrossRef](#)]

7. Orlenko, E.V.; Ershova, E.V.; Orlenko, F.E. Invariant exchange perturbation theory for multicenter systems and its application to the calculation of magnetic chains in manganites. *J. Exp. Theor. Phys.* **2013**, *117*, 674–690. [[CrossRef](#)]
8. Fiebig, M.; Fröhlich, D.; Kohn, K.; Leute, S.; Lottermoser, T.; Pavlov, V.V.; Pisarev, R.V. Determination of the magnetic symmetry of hexagonal manganites by second harmonic generation. *Phys. Rev. Lett.* **2000**, *84*, 5620–5623. [[CrossRef](#)]
9. Rai, R.C.; Cao, J.; Musfeldt, J.L.; Kim, S.B.; Cheong, S.W.; Wei, X. Spin-charge coupling and the high-energy magnetodielectric effect in hexagonal HoMnO₃. *Phys. Rev. B* **2007**, *75*, 184414. [[CrossRef](#)]
10. Souchkov, A.B.; Simpson, J.R.; Quijada, M.; Ishibashi, H.; Hur, N.; Ahn, J.S.; Cheong, S.W.; Millis, A.J.; Drew, H.D. Exchange interaction effects on the optical properties of LiMnO₃. *Phys. Rev. Lett.* **2003**, *91*, 027203. [[CrossRef](#)]
11. Choi, W.S.; Kim, D.G.; Seo, S.S.A.; Moon, S.J.; Lee, D.; Lee, J.H.; Lee, H.S.; Cho, D.Y.; Lee, Y.S.; Murugavel, P.; et al. Electronic structures of hexagonal RMnO₃ (R = Gd, Tb, Dy, and Ho) thin films: Optical spectroscopy and first-principles calculations. *Phys. Rev. B* **2008**, *77*, 045137. [[CrossRef](#)]
12. Choi, W.S.; Moon, S.J.; Seo, S.S.A.; Lee, D.; Lee, J.H.; Murugavel, P.; Noh, T.W.; Lee, Y.S. Optical spectroscopic investigation on the coupling of electronic and magnetic structure in multiferroic hexagonal RMnO₃ (R = Gd, Tb, Dy, and Ho) thin films. *Phys. Rev. B* **2008**, *78*, 054440. [[CrossRef](#)]
13. Degenhardt, C.; Fiebig, M.; Fröhlich, D.; Lottermoser, T.; Pisarev, R.V. Nonlinear optical spectroscopy of electronic transitions in hexagonal manganites. *Appl. Phys. B* **2001**, *73*, 139–144. [[CrossRef](#)]
14. Dagotto, E.; Hotta, T.; Moreo, A. Colossal magnetoresistant materials: The key role of phase separation. *Phys. Rep.* **2001**, *344*, 1–153. [[CrossRef](#)]
15. Loktev, V.M.; Pogorelov, Y.G. Peculiar physical properties and the colossal magnetoresistance of manganites. *Low Temp. Phys.* **2000**, *26*, 171–193. [[CrossRef](#)]
16. Orlova, T.S.; Laval, J.Y.; Monod, P.; Bassoul, P.; Noudem, J.G.; Orlenko, E.V. Influence of Mn-site doping on charge and orbital ordering in La_{1/3}Ca_{2/3}Mn_{1-y}M_yO₃ manganites (M = Ni, Ga). *Phys. Rev. B* **2009**, *79*, 134407. [[CrossRef](#)]
17. Lee, S.; Pirogov, A.; Kang, M.; Jang, K.H.; Yonemura, M.; Kamiyama, T.; Cheong, S.W.; Gozzo, F.; Shin, N.; Kimura, H.; et al. Giant magneto-elastic coupling in multiferroic hexagonal manganites. *Nature* **2008**, *451*, 805–808. [[CrossRef](#)]
18. Lee, S.; Pirogov, A.; Han, J.H.; Park, J.G.; Hoshikawa, A.; Kamiyama, T. Direct observation of a coupling between spin, lattice and electric dipole moment in multiferroic YMnO₃. *Phys. Rev. B* **2005**, *71*, 180413. [[CrossRef](#)]
19. Vermette, J.; Jandl, S.; Mukhin, A.A.; Ivanov, V.Y.; Balbashov, A.; Gospodinov, M.M.; Pinsard-Gaudart, L. Raman study of the antiferromagnetic phase transitions in hexagonal Y MnO₃ and LuMnO₃. *J. Phys. Condens. Matter* **2010**, *22*, 356002. [[CrossRef](#)]
20. Litvinchuk, A.P.; Iliev, M.N.; Popov, V.N.; Gospodinov, M.M. Raman and infrared-active phonons in hexagonal HoMnO₃ single crystals: Magnetic ordering effects. *J. Phys. Condens. Matter* **2004**, *16*, 809–819. [[CrossRef](#)]
21. Basistyy, R.; Stanislavchuk, T.N.; Sirenko, A.A.; Litvinchuk, A.P.; Kotelyanskii, M.; Carr, G.L.; Lee, N.; Wang, X.; Cheong, S.W. Infrared-active optical phonons and magnetic excitations in the hexagonal manganites RMnO₃, (R = Er, Tm, Yb, and Lu). *Phys. Rev. B* **2014**, *90*, 024307. [[CrossRef](#)]
22. Wu, K.H.; Hsu, T.Y.; Shih, H.C.; Chen, Y.J.; Luo, C.W.; Uen, T.M.; Lin, J.Y.; Juang, J.Y.; Kobayashi, T. Ultrafast optical probes of polaron dynamics in La_{0.7}Ca_{0.3}MnO₃ thin films. *J. Appl. Phys.* **2009**, *105*, 043901. [[CrossRef](#)]
23. Luo, C.W.; Chen, M.H.; Chen, S.P.; Wu, K.H.; Juang, J.Y.; Lin, J.Y.; Uen, T.M.; Gou, Y.S. Spatial symmetry of the superconducting gap of YBa₂Cu₃O_{7-δ} obtained from femtosecond spectroscopy. *Phys. Rev. B* **2003**, *68*, 220508. [[CrossRef](#)]
24. Luo, C.W.; Wu, I.H.; Cheng, P.C.; Lin, J.Y.; Wu, K.H.; Uen, T.M.; Juang, J.Y.; Kobayashi, T.; Wen, Y.C.; Huang, T.W.; et al. Ultrafast dynamics and phonon softening in Fe_{1+y}Se_{1-x}Te_x single crystals. *New J. Phys.* **2012**, *14*, 103053. [[CrossRef](#)]
25. Chen, H.J.; Wu, K.H.; Luo, C.W.; Uen, T.M.; Juang, J.Y.; Lin, J.Y.; Kobayashi, T.; Yang, H.D.; Sankar, R.; Chou, F.C.; et al. Phonon dynamics in Cu_xBi₂Se₃ (x = 0, 0.1, 0.125) and Bi₂Se₂ crystals studied using femtosecond spectroscopy. *Appl. Phys. Lett.* **2012**, *101*, 121912. [[CrossRef](#)]
26. Luo, C.W.; Chung Cheng, P.; Wang, S.H.; Chiang, J.C.; Lin, J.Y.; Wu, K.H.; Juang, J.Y.; Chareev, D.A.; Volkova, O.S.; Vasiliev, A.N. Unveiling the hidden nematicity and spin subsystem in FeSe. *NPJ Quantum Mater.* **2017**, *2*, 32. [[CrossRef](#)]
27. Qi, J.; Yan, L.; Zhou, H.D.; Zhu, J.X.; Trugman, S.A.; Taylor, A.J.; Jia, Q.X.; Prasankumar, R.P. Coexistence of coupled magnetic phases in epitaxial TbMnO₃ films revealed by ultrafast optical spectroscopy. *Appl. Phys. Lett.* **2012**, *101*, 122904. [[CrossRef](#)]
28. Wu, K.H.; Chen, H.J.; Hsieh, C.C.; Luo, C.W.; Uen, T.M.; Lin, J.Y.; Juang, J.Y. Epitaxial-strain effects on electronic structure and magnetic properties of hexagonal YMnO₃ thin films studied by femtosecond spectroscopy. *J. Supercond. Nov. Magn.* **2013**, *26*, 801. [[CrossRef](#)]
29. Shih, H.C.; Lin, T.H.; Luo, C.W.; Lin, J.Y.; Uen, T.M.; Juang, J.Y.; Wu, K.H.; Lee, J.M.; Chen, J.M.; Kobayashi, T. Magnetization dynamics and the Mn³⁺d–d excitation of hexagonal HoMnO₃ single crystals using wavelength-tunable time-resolved femtosecond spectroscopy. *Phys. Rev. B* **2009**, *80*, 024427. [[CrossRef](#)]
30. Wu, K.H.; Chen, H.J.; Chen, Y.T.; Hsieh, C.C.; Luo, C.W.; Uen, T.M.; Juang, J.Y.; Lin, J.Y.; Kobayashi, T.; Gospodinov, M. Marked enhancement of Néel temperature in strained YMnO₃ thin films probed by femtosecond spectroscopy. *EPL (Europhys. Lett.)* **2011**, *94*, 27006. [[CrossRef](#)]
31. Shih, H.C.; Chen, L.Y.; Luo, C.W.; Wu, K.H.; Lin, J.Y.; Juang, J.Y.; Uen, T.M.; Lee, J.M.; Chen, J.M.; Kobayashi, T. Ultrafast thermoelastic dynamics of HoMnO₃ single crystals derived from femtosecond optical pump–probe spectroscopy. *New J. Phys.* **2011**, *13*, 053003. [[CrossRef](#)]

32. Fröhlich, D.; Leute, S.; Pavlov, V.V.; Pisarev, R.V. Nonlinear optical spectroscopy of the two-order-parameter compound YMnO_3 . *Phys. Rev. Lett.* **1998**, *81*, 3239–3242. [[CrossRef](#)]
33. Wang, Y.T.; Luo, C.W.; Kobayashi, T. Understanding multiferroic hexagonal manganites by static and ultrafast optical spectroscopy. *Adv. Condens. Matter Phys.* **2013**, *2013*, 104806. [[CrossRef](#)]
34. Kobayashi, T.; Baltuska, A. Sub-5 fs pulse generation from a noncollinear optical parametric amplifier. *Meas. Sci. Technol.* **2002**, *13*, 1671–1682. [[CrossRef](#)]
35. Shirakawa, A.; Sakane, I.; Takasaka, M.; Kobayashi, T. Sub-5-fs visible pulse generation by pulse-front-matched noncollinear optical parametric amplification. *Appl. Phys. Lett.* **1999**, *74*, 2268–2270. [[CrossRef](#)]
36. Luo, C.W.; Wang, Y.T.; Yabushita, A.; Kobayashi, T. Ultrabroadband time-resolved spectroscopy in novel types of condensed matter. *Optica* **2016**, *3*, 82–92. [[CrossRef](#)]
37. Kimel, A.V.; Pisarev, R.V.; Bentivegna, F.; Rasing, T. Time-resolved nonlinear optical spectroscopy of Mn^{3+} ions in rare-earth hexagonal manganites RMnO_3 ($R = \text{Sc}, \text{Y}, \text{Er}$). *Phys. Rev. B* **2001**, *64*, 201103. [[CrossRef](#)]
38. Satoh, T.; Van Aken, B.B.; Duong, N.P.; Lottermoser, T.; Fiebig, M. Ultrafast spin and lattice dynamics in antiferromagnetic Cr_2O_3 . *Phys. Rev. B* **2007**, *75*, 155406. [[CrossRef](#)]
39. Sheu, Y.M.; Trugman, S.A.; Park, Y.S.; Lee, S.; Yi, H.T.; Cheong, S.W.; Jia, Q.X.; Taylor, A.J.; Prasankumar, R.P. Ultrafast carrier dynamics and radiative recombination in multiferroic BiFeO_3 . *Appl. Phys. Lett.* **2012**, *100*, 242904. [[CrossRef](#)]
40. Talbayev, D.; Lee, J.; Trugman, S.A.; Zhang, C.L.; Cheong, S.W.; Averitt, R.D.; Taylor, A.J.; Prasankumar, R.P. Spin-dependent polaron formation dynamics in $\text{Eu}_{0.75}\text{Y}_{0.25}\text{MnO}_3$ probed by femtosecond pump-probe spectroscopy. *Phys. Rev. B* **2015**, *91*, 064420. [[CrossRef](#)]
41. Fukunaga, K.; Hashimoto, M.; Kunugita, H.; Kamimura, J.; Kikuchi, A.; Kishino, K.; Ema, K. Energy- and density-dependent dynamics of photoexcited carriers in InN films. *Appl. Phys. Lett.* **2009**, *95*, 232114. [[CrossRef](#)]
42. Wall, S.; Prabhakaran, D.; Boothroyd, A.T.; Cavalleri, A. Ultrafast coupling between light, coherent lattice vibrations, and the magnetic structure of semicovalent LaMnO_3 . *Phys. Rev. Lett.* **2009**, *103*, 097402. [[CrossRef](#)] [[PubMed](#)]
43. Nakayama, M.; Furukawa, Y.; Maeda, K.; Yoshimura, T.; Uga, H.; Fujimura, N. Correlation between the intra-atomic Mn^{3+} photoluminescence and antiferromagnetic transition in an YMnO_3 epitaxial film. *Appl. Phys. Express* **2014**, *7*, 023002. [[CrossRef](#)]
44. Ogasawara, T.; Ohgushi, K.; Tomioka, Y.; Takahashi, K.S.; Okamoto, H.; Kawasaki, M.; Tokura, Y. General features of photoinduced spin dynamics in ferromagnetic and ferrimagnetic compounds. *Phys. Rev. Lett.* **2005**, *94*, 087202. [[CrossRef](#)] [[PubMed](#)]
45. Toulouse, C.; Liu, J.; Gallais, Y.; Measson, M.A.; Sacuto, A.; Cazayous, M.; Chaix, L.; Simonet, V.; de Brion, S.; Pinsard-Godart, L.; et al. Lattice and spin excitations in multiferroic $h\text{-YMnO}_3$. *Phys. Rev. B* **2014**, *89*, 094415. [[CrossRef](#)]
46. Fiebig, M.; Degenhardt, C.; Pisarev, R.V. Interaction of frustrated magnetic sublattices in ErMnO_3 . *Phys. Rev. Lett.* **2001**, *88*, 027203. [[CrossRef](#)] [[PubMed](#)]